Pergamon

Cement and Concrete Research, Vol. 28, No. 9, pp. 1223–1235, 1998

0008-8846/98 $19.00 + .00

PII S0008-8846(98)00137-9

WEATHERING OF IRON SULFIDES AND CONCRETE ALTERATION: THERMODYNAMIC MODEL AND OBSERVATION IN DAMS FROM CENTRAL PYRENEES, SPAIN

C. Ayora,* S. Chinchón,[1]† A. Aguado,‡ and F. Guirado‡
*Instituto de Ciencias de la Tierra. c/Martí i Franqués s/n, 08028 Barcelona, España
†Departamento de Construcciones Arquitectónicas, Universidad de Alicante, E-03080 Alicante, España
‡Departamento de Ingeniería de la Construcción, Universidad Politécnica de Catalunya, Catalunya, España

(Received October 29, 1996; in final form January 23, 1998)

PUBLISHER'S NOTE

This article was originally published in *Cement and Concrete Research*, Vol. 28, No. 4, pp. 591–603, with incorrect placement of figures. This version completely supersedes the previously published version, which should be disregarded. The publishers apologize to the author for the error.

ABSTRACT

The concrete of the Graus and Tabescan dams present significant durability problems. The cement paste is altered to expansive phases such as ettringite and gypsum, following fractures and aggregate-paste interfaces. The alteration is initially attributed to the acidic solution produced by the weathering of the pyrrhotite contained in the aggregate fragments. A chemical model, based on ion association and thermodynamic equilibrium, permits the calculation of the mass transfer between the solids and the pore solution, and the prediction of the progress of the acidic attack. The results of the calculations have been compared with the alteration features observed in concrete of these dams. Despite the simplifications, this model is able to predict the observed alteration stages, and confirms the hypothesis of acidic-sulfatic alteration of the cement. © *1998 Elsevier Science Ltd*

Introduction

The construction of a dam involves large volumes of concrete, and therefore a considerable amount of rock is also required for use as aggregates. Economic constraints require aggregates to be found in the immediate construction area. This is particularly true in the case of

[1]To whom correspondence should be addressed.

dams, often located in remote regions, where the aggregates come from the surrounding rocks.

It is well established that not all rocks are suitable for use as aggregates in concrete (1). Those aggregates that due to weathering or to reactions with cement give rise to compounds of greater volume are not allowed. However, the formation of expansive compounds in the concrete due to the use of sulfide-bearing aggregates has rarely been described in the literature (2,3).

The dams of Graus and Tabescán are gravity dams built in the Ribera de Cardós and Tabescán rivers respectively, in the Central Pyrenees, Spain. They both contain notable examples of concrete degradation. In 1992, the propietor of the dams, the electric power company FECSA, contracted a research group from the Universitat Politècnica de Catalunya (UPC) to diagnose the factors that account for this concrete alteration (4). Given the difficulties in reproducing such processes in the laboratory over a short time span, a numerical simulation of the concrete degradation processes was sought. The predictions of the model were compared with both the mineralogy and textures observed in samples from the dams. The sequence of the stages and the present extent of degradation in the concrete of the dams was subsequently established.

Concrete Deterioration

Concrete can be considered as a solid volume, made up of a paste of hydrated cement and rock fragments or aggregates. The hydration of Portland cement, used in the Graus and Tabescán dams, gives the following compounds: hydrated calcium silicates, CSH, and portlandite, CH, formed by the hydration of bi- and tri-calcium silicates, C_2S and C_3S ($C = CaO$; $S = SiO_2$; $H = H_2O$); and hydrated calcium aluminates formed by the hydration of calcium aluminates. These compounds partly combine with the gypsum added to the clinker to form ettringite, $C_6A\bar{S}_3H_{32}$ ($\bar{S} = SO_3$). We call this a primary ettringite, in order to distinguish it from the ettringite formed later from alteration processes.

The aggregates of the concrete used in the dams studied are rock fragments ranging in size from 1 to 100 mm. The rocks are schists extracted from the dams' surroundings. They are mainly formed by quartz, muscovite, chlorite, and albite. The schists may contain minor amounts of pyrrhotite (Fe_7S_8) as disseminated crystals and millimeter-size veinlets. The total sulfur content in the rock is up to 0.8 wt.% S (4). Additional expansive minerals, such as clays, zeolites, and graphite were not determined in significant amounts. Weathering was observed in some rock outcrops close to the dams. Here, abundant jarosite, iron hydroxide, gypsum, and pickeringite were identified. This weathering is related to the oxidation of pyrrhotite, whereas significant dissolution of silicates and neoformation of clays (such as kaolinite) were not observed.

An important cracking process is observed in the Graus and Tabescán dams. Samples of concrete were collected from the surface, and from drill cores of up to 3 m from the surface. The surfaces of the sawn hand specimens were initially treated with phenolphtaleine. Most of the cement mass was stained a purple color, indicating a pH higher than 12.0 in the pore water. Colorless areas surrounding fractures and the aggregate-paste interface are clearly apparent (Fig. 1). These areas are interpreted as having pore water with lower pH values, which is attributed as due to the cement chemical alteration. Eleven samples from these particular areas were collected for further mineralogical and textural determination.

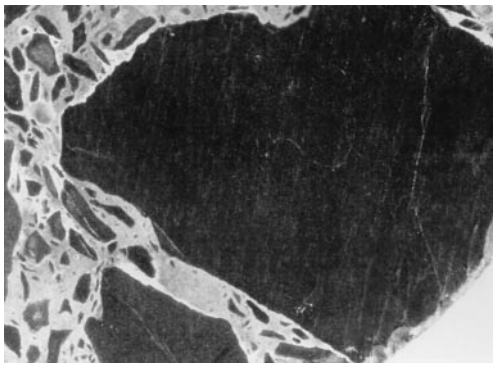

FIG. 1.
Surface of drill core of concrete from Graus dam after staining with phenolphthalein. The dark color of the paste (purple) corresponds to unaltered cement paste. The white zones (unstained), following a fracture and the aggregate-paste interface, correspond to chemically altered cement paste.

The mineralogy and textures of the altered cement from fractures and aggregate-paste interfaces, were determined using X-ray diffraction (XRD) and Scanning Electron Microscopy (SEM), coupled with Energy Dispersive System (EDS) of microanalysis. Ettringite was identified by XRD, in all the samples studied. Exhaustive textural determination by SEM was oriented to distinguishing the presence of ettringite due to alteration processes (secondary), from that already in the hydrated cement (primary). Ettringite was currently observed as needle-shape crystals filling cavities and fractures in the cement paste (Figs. 2 and 3). These textures indicate that the ettringite crystals formed as an alteration phase. The EDS determination of calcium, aluminum, and sulfur as constituents of the crystals confirmed the identification of ettringite.

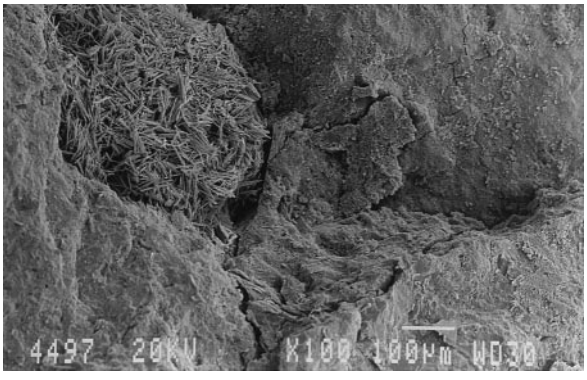

FIG. 2.
Scanning electron micrograph of a cavity in the paste, filled with newly formed ettringite, corresponding to alteration of the cement paste.

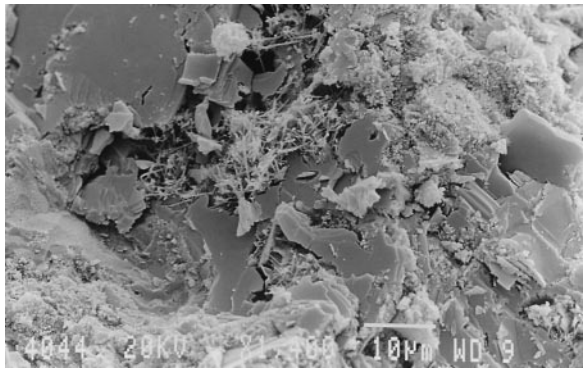

FIG. 3.
Scanning electron micrograph of a fracture in the aggregate (platy crystals of portlandite) filled with newly formed ettringite.

Radial aggregates of needle-shape crystals of gypsum were also commonly found in the colorless altered cement. Calcium and sulfur were identified by EDS as being constituents of the crystals. As in the case of ettringite, the gypsum crystals fill pores and cavities of the cement paste, suggesting that their formation is an alteration phase (Fig. 4). We observed that gypsum crystals grew at the expense of ettringite crystals (Fig. 5). This texture, together with the observation that initial portlandite is practically absent when gypsum is present, suggests that gypsum postdates ettringite as a more advanced alteration phase.

The acidic alteration could also affect the mineral constituents of the aggregate rock. Therefore, a complementary study of the rock in the surrounding of altered pyrrhotite was also carried out by optical microscopy (reflected and transmitted light) and SEM-EDS. The

FIG. 4.
Scanning electron micrograph of a cavity in the paste filled with gypsum, corresponding to an advanced stage of alteration.

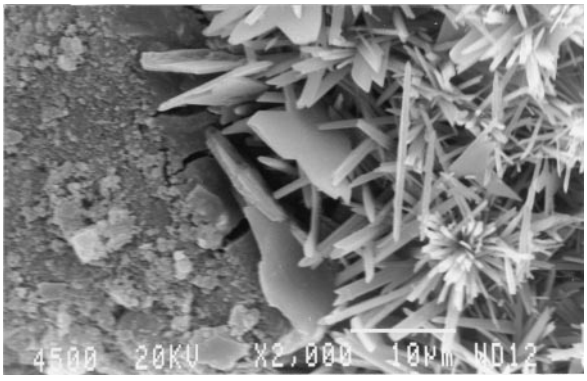

FIG. 5.
Interface of aggregate-paste constitued by portlandite (platy crystals) and newly-formed ettringite (needle-shape crystals). Gypsum (radial aggregates of needle-shape crystals) grows at the expense of ettringite crystals.

rock-forming silicates did not show evidence of significant chemical alteration in relation to the oxidation of the pyrrhotite grains. Only amorphous iron hydroxide was occasionally observed as a coat on the silicate surfaces. The lack of silicate alteration is consistent with the hydrolysis rates of silicates at ambient temperatures (10^{-11} to 10^{-14} mol m^{-2} s^{-1}, (5,6)). These rates are between 2 and 5 orders of magnitude slower than the oxidation rate of pyrrhotite (10^{-9} mol m^{-2} s^{-1}, (7)). The lack of significant silicate alteration is also evidenced by the absence of neoformed clays (such as kaolinite) in the rock outcrops close to the dams, and affected by intensive sulfide weathering.

The Thermodynamic Model

Conceptual Model

A simplified representation of the concrete system and the acidic alteration is required to make the calculations possible. According to our estimations (4), the hydrated cement paste is assumed to be made up of approximately 45 vol. % of colloidal particles of low crystallinity (tobermoritic gel), 15 vol. % of CH, 10 vol. % of primary ettringite, 10 vol. % of hydrated calcium aluminates not combined with gypsum (arbitrarily represented as C_4AH_{19}), and 20 vol. % porosity. The Al^{3+} structural sites may be partially replaced by Fe^{3+}, but this possibility has not been considered in our study. Following the lack of significant alteration of the rock silicates, the aggregate was considered to be inert in the calculations.

The pyrite oxidation process to give sulfuric acid has been investigated in detail (8,9). Despite being the second most abundant sulfide in the lithosphere, very few experiments have been carried out on pyrrhotite oxidation. According to (7), the oxidation of pyrrhotite by oxygen can be written as:

$$Fe_{1-x}S + \left(2 - \frac{x}{2}\right)O_2 + xH_2O = (1 - x)\,Fe^{2+} + SO_4^{2-} + 2x\,H^+$$

where x can vary from 0 to 0.125. The subsequent oxidation of Fe^{2+} and precipitation of Fe^{3+}-hydroxide may increase the acid production:

$$(1 - x)\,Fe^{2+} + \left(\frac{1 - x}{4}\right)O_2 + \left(\frac{5 - 5x}{2}\right)H_2O = (1 - x)\,Fe(OH)_3 + (2 - 2x)\,H^+$$

where 1 mol of pyrrhotite may generate up 1 mol of sulfuric acid. The increase in the chemical potential of the $SO_4^{=}$ and H^+ of the interstitial water, modifies the initial conditions of equilibrium and initiates a process of mass transfer between the solids and the water. As a consequence, the dissolution of the initial solids, the formation of new associations of solids incorporating $SO_4^{=}$ and H^+, and the variation in the solute concentration in the solution, take place. Because Fe was not included in the calculations, the formation of iron hydroxide, a mineral present in the altered samples, was not considered.

Description of the Calculations

A model based on equilibrium thermodynamics allows us to predict the concentration of solutes in the solution and the mass transfer to/from the solid phases. This type of model is currently used in geochemistry to simulate the progress of chemical reactions involved in natural processes (10–12, among others). A similar model applied to the description of the cement-water interaction has recently been presented by Reardon (13). In his model, the activity coefficients accounting for the non-ideal behavior of the ions in the solution were calculated using the Pitzer's ion-ion interaction model. These calculations can be extended to highly concentrated brines, but the interaction coefficients between ions must be previously deduced from experiments. In the model presented here, the non-ideal behavior is calculated assuming the existence of aqueous species formed by association of single ions. The activity coefficients of the ions and associations are calculated from a fundamental equation (Debye-Hückel formula), and are only dependent on the ionic strength of the solution, regardless of the ions present. As a consequence, the ion-association model presented here is for more general application than a ion-interaction model, although it is not useful for solutions with ionic strengths higher than 0.1. The low concentrations expected in the pore water in cement (see later) enable us to use the proposed ion-association model.

For each chemical component, among the set of N_c components required to describe the system (H_2O, Al, Si, Ca, OH^-, SO_4), a mass balance equation is formulated:

$$t_i = c_i + \sum_{j=1}^{N_x} V_{ji}\,x_j \tag{1}$$

where t_i is the total concentration (mol/kg water) of the ith component in the system; c_i is the concentration of an aqueous species of the ith component arbitrarily selected, here named the primary species (one for each component); N_x is the number of the remaining non-primary species in solution; x_j is the concentration (mol/kg) of the jth species; n_{ji} is the stoichiometric coefficient of the ith primary species in the dissociation reaction of the jth species; N_p is the number of solid phases involved in the reactions; p_m is the amount (mol/kg) of the mth solid

phase and n_{mi} the stoichiometric coefficient of the *i*th primary species in the dissolution reaction of the *m*th solid phase.

Assuming thermodynamic equilibrium between the aqueous species in solution, N_x mass-action-law equations can be formulated, one for each non-primary aqueous species:

$$K_j = x_j^{-1}\gamma_j^{-1}\prod_{i=1}^{N_c} c_i^{yji}\gamma_i^{yji} \qquad j = 1 \ldots N_x \tag{2}$$

where K_j is the equilibrium constant of the dissociation reaction of the *j*th species, and *g* is the thermodynamic activity coefficient of the aqueous species, calculated according to the extended Debye-Hückel formula (11).

Similarly, assuming thermodynamic equilibrium between the solution and the solid phases, N_p mass-action-law equations can be formulated, one for each solid present in the system:

$$K_m = \prod_{i=1}^{N_c} c_i^{vmi}\gamma_i^{vmi} \qquad m = \ldots N_p \tag{3}$$

where K_m is the equilibrium constant of the dissolution reaction of the *m*th solid phase. The concentration and activity coefficients of pure solids are considered equal to unity.

Equations 1, 2, and 3 form a system of $N_c + N_x + N_m$ equations with the same number of unknowns, c_i, x_j and p_m. The equations are non-linear and the solution requires numerical methods such as Newton-Raphson iterations (10). The list of primary species, the chemical reactions considered in the system, and their equilibrium constants are listed in Table 1.

The Solubility of CSH

CSH is the most important constituent of hydrated Portland cement. More than a pure phase with a well-defined crystalline structure, CSH can be considered as a gel phase. This fact leads to two important characteristics: there are several forms of CSH, and the Ca/Si ratio of CSH varies with the Ca/Si ratio of the solution (17,18). These characteristics prevent the use of a unique equilibrium constant for CSH in the dissolution reactions (Table 1).

Among the different CSH forms we have considered the most stable one, which corresponds to a tobermorite-like structure formed in the advanced stages of hydration (18). The Ca/Si ratio of the solid phase has been calculated from the Ca/Si ratio of the solution following the method proposed by Gartner and Jennings (18). Because the aqueous speciation model used in our calculations (Table 1) is similar to that used by the former authors, the Ca/Si ratio of CSH has been calculated directly from their data (ref. 18, Table 3, curve 2, $K_5 = K_6 = 0$). The resulting variation of the Ca/Si ratio of CSH and that of the solution is plotted in Figure 6, and can be approximated by Equation 4:

$$(Ca/Si)_{CSH} = 1.650 - 0.654x + 0.107x^2 \tag{4}$$

where x is log $(Ca/Si)_{SOL}$.

The variation of the equilibrium constant of the dissolution reaction of CSH has been calculated from the composition of the solutions in equilibrium with the tobermorite-like CSH (ref. 18, Table 3, curve 2, $K_5 = K_6 = 0$). The activity of the aqueous species involved in the dissolution reaction (a_{Ca2+}, a_{H4SiO4}, a_{OH-}, a_{H2O}) has been obtained from the measured solute concentration, using the system of $N_c + N_x$ equations formed by Eq. 1 and 2 ($p_m = 0$ and t_i being the solute concentration), and the thermodynamic data for aqueous speciation

TABLE 1
Thermodynamic data (25°C) for chemical reactions involved in the calculations.

Primary species:
H_2O, OH^-, Ca^{2+}, $H_4SiO_4^o$, $Al(OH)_4^-$, $SO_4^=$

Non-primary aqueous species:	log K*
$H^+ = H_2O - OH^-$	14.00
$H_3SiO_4^- = H_4SiO_4^o - H_2O + OH^-$	−4.23
$H_2SiO_4^= = H_4SiO_4^o - 2H_2O + 2OH^-$	−6.58
$Ca(OH)^+ = Ca^{2+} + OH^-$	−1.22
$CaSO_4^o = Ca^{2+} + SO_4^=$	−2.43
$Al(OH)_3^o = Al(OH)_4^- - OH^-$	6.49
$Al(OH)_2^+ = Al(OH)_4^- - 2OH^-$	14.62

Solid phases:	log K*	Molar Vol. (cm^3/mol)
$CaSiO_3 \times H_2O = Ca^{2+} + H_4SiO_4^o - 2H_2O + 2OH^-$	†	57.36‡
$Ca_4Al_2O_7 \times 19H_2O = 4Ca^{2+} + 2Al(OH)_4^- + 12H_2O + 60H^-$	−27.94	371.44‡
$Ca(OH)_2 = Ca^{2+} + 2OH^-$	−5.21	33.06§
$CaSO_4 \times 2H_2O = Ca^{2+} + SO_4^= + 2H_2O$	−4.65	74.69§
$Al(OH)_3 = Al(OH)_4^- - OH^-$	−1.02	31.96§
$SiO_2(am) = H_4SiO_4^o - 2H_2O$	−2.71	29.00¶
$Ca_6Al_2O_6(SO_4)_3 \times 32H_2O = 6Ca^{2+} + 2Al(OH_4^- + 3SO_4^= + 26H_2O + 4OH^-$	−44.00	704.82‡

*See text for discussion.
†Calculated from thermodynamic data referred to in [14]: $\log K = -(SG_{PRODUCTS} - SG_{REACTANTS})/(2.303RT)$.
‡Calculated from density data referred to in [16].
§Data from [15].
¶Data from EQ3NR database [12].

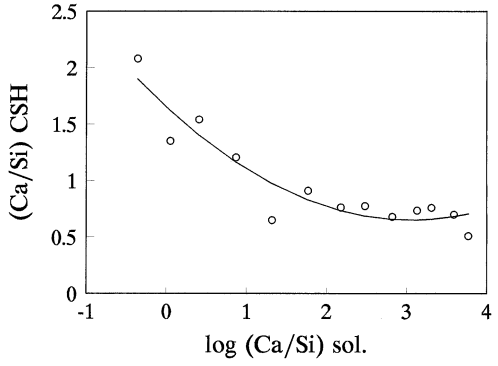

FIG. 6.
Compositional variation for CSH with respect to the composition of the solution. Data from Gartner and Jennings (ref. 18, Table 3, curve 2, $K_5 = K_6 = 0$).

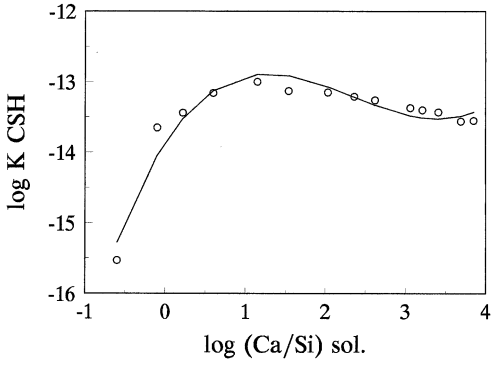

FIG. 7.

Variation of the equilibrium constant for the CSH dissolution reaction (Table 1) with respect to the composition of the solution. Data from Gartner and Jennings (ref. 18, Table 3, curve 2, $K_5 = K_6 = 0$).

is referred to in Table 1. The a_{OH-} values have been obtained from the chemical potential of the $Ca(OH)_2$ component (m_C in ref. 18, Table 3, curve 2, $K_5 = K_6 = 0$), and the a_{Ca2+} values (according to ref. 18, Eq. 10). The variation of the equilibrium constant for CSH dissolution with the Ca/Si ratio of the solution is plotted in Figure 7, and can approximated by Equation 5:

$$\log K_{CSH} = -13.863 + 1.743x - 0.937x^2 + 0.134x^3 \quad (5)$$

where x is $\log (Ca/Si)_{SOL}$.

Model Application and Discussion

According to the proportions of aggregates, cement, and water originally used in the concrete of the Graus and Tabescán dams (4), an idealized block of 1 dm^3 of concrete was assumed to be formed by 850 cm^3 of aggregate and 150 cm^3 of cement paste. From the porosity and the volume proportion of solid phases in the cement referred to above (and the molar volumes listed in Table 1), the 150 cm^3 of cement paste can be considered as being initially formed by 1.17 mol of CSH, 0.04 mol of C_4AH_{19}, 0.68 mol of portlandite, and 0.02 mol of primary ettringite. The same proportions normalized to 1 kg of water (density of the solution assumed 1 g/cm^3) are listed in Table 2. The solute concentration in the initial pore water was calculated to be in equilibrium with the four initial solid phases (Table 2).

In order to simulate the alteration features observed in the studied dams, an excess of sulfuric acid was added to the system. The availability of sulfuric acid from the oxidation of pyrrhotite present in the aggregates will be discussed later. The alteration of cement was simulated by running the chemical model successively, each time increasing the t_{SO4} value and decreasing the t_{OH} value of Eq. 1, in the adequate proportion of 1:2. The system evolves to a new equilibrium stage. The hypothesis of thermodynamic equilibrium implicitly assumes that the dissolution/precipitation rates of the cement/alteration phases are higher than the rate

TABLE 2
Initial conditions for the calculation of the alteration of cement by sulfuric acid.

Pore water:	solute (mol/kg)	
Si	4.50×10^{-5}	
Ca	1.80×10^{-2}	
Al	1.12×10^{-5}	
S	1.00×10^{-4}	
pH	12.48	
Solid phases:	mol/kg water	log SI*
CSH	39.23	0.00
C_4AH_{19}	1.35	0.00
portlandite	22.69	0.00
ettringite	0.71	0.00
gypsum	0.00	−7.83
gibbsite	0.00	−2.50
amorph. silica	0.00	−6.34

*SI = ion activity product/K_{eq}.

of pyrrhotite oxidation. Therefore, the rate of pyrrhotite oxidation is considered to be the limiting rate of the overall alteration process.

The evolution of the solute concentration with respect to the progress of alteration is plotted in Figure 8. New solid phases were added to the system as the solution became supersaturated with respect to this phase. The solid phases exhausted by dissolution were removed from the system. In order to compare the observations, the evolution of the amount of solid phases is plotted with respect to pH in Figures 9 and 10. These results are comparable to those presented by Reardon (13) for a similar case but using a different thermodynamic

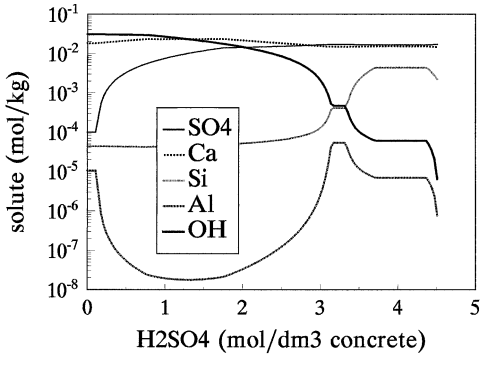

FIG. 8.
Compositional variation of the pore water in cement as acidic-sulfatic alteration progresses. A 15% vol. cement proportion is assumed for the concrete.

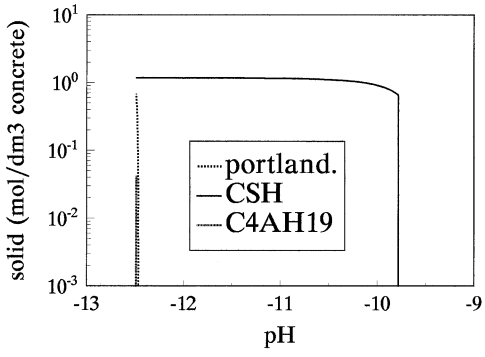

FIG. 9.
Dissolved mass of solids initially present in cement with respect to pH variation. A 15% vol. cement proportion is assumed for the concrete.

model. The evolution of the a_{OH^-} values (Fig. 9) shows a progressive decrease in the pH of the interstitial water, with three stages of invariant pH. At a pH of 12.5 the dissolution of portlandite and C_4AH_{19} takes place (Fig. 10). The increase of Ca^{2+} and $Al(OH)_4^-$ from dissolution, together with the addition of $SO_4^{=}$, results in the precipitation of secondary ettringite (Fig. 10), according to the reaction:

$$2Ca(OH)_2 + Ca_4Al_2O_7{\cdot}19H_2O + 8H_2O + 3SO_4^{=} + 6H^+ = Ca_6Al_2O_6(SO_4)_3 32H_2O$$

The exhaustion of C_4AH_{19} limits the supply of $Al(OH)_4^-$ and prohibits the formation of ettringite. Hence the dissolution of portlandite is the only reaction to take place. The predicted association coincides with observations, where portlandite coexists with newly

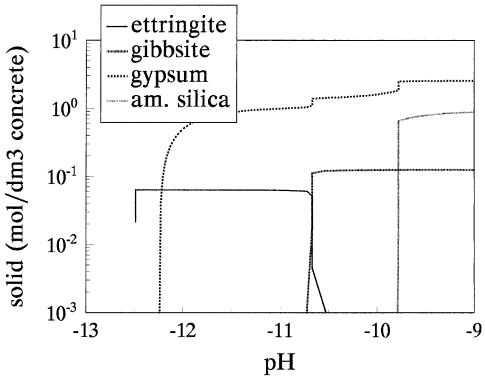

FIG. 10.
Dissolved/precipitated mass of solids formed by alteration of cement with respect to pH variation. A 15% vol. cement proportion is assumed for the concrete.

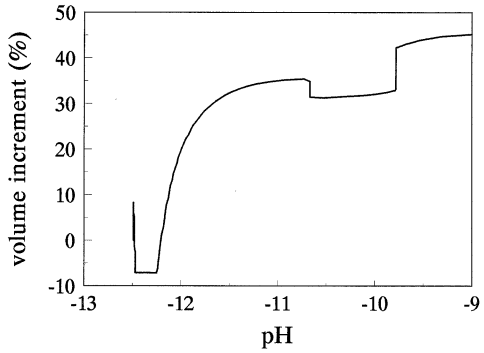

FIG. 11.
Variation of volume, relative to the total volume of solids in the cement paste due to the dissolution/precipitation of solid phases. A 15% vol. cement proportion is assumed for the concrete.

formed ettringite in some altered interfaces between the aggregates and the paste. The dissolution of portlandite consumes the added H^+ and the pH value remains invariant at 12.5.

Once the portlandite is exhausted the addition of H^+ makes the pH drop. The addition of $SO_4^=$ saturates the solution with respect to gypsum, which starts to form at a pH of 12.25. In the altered zones, the pH values lower than 12.5 are beautifully shown by the lack of stain with phenophtaleine. This test can be carried out in the field. However, fresh samples of concrete are required, because surface carbonation of portlandite due to the atmospheric CO_2 can also decrease the pH of the pore water.

At a pH of 10.7, ettringite dissolves and the formation of gibbsite and additional gypsum takes place:

$$Ca_6Al_2O_6(SO_4)_3{\cdot}32H_2O + 4SO_4^= + 8H^+ = 4CaSO_4{\cdot}2H_2O + 2\,Al(OH)_3 + 12H_2O$$

This reaction consumes the added H^+ and the pH remains constant until the total consumption of ettringite (both primary and secondary) occurs. In accordance with predictions the presence of gypsum is observed replacing ettringite in the altered zones. Gibbsite, however, has not been detected by X-ray diffraction, maybe due to the formation of an amorphous aluminum hydroxide.

Once ettringite is exhausted, the pH drops. At a pH of 9.8, CSH dissolves. The increase in $H_4SiO_4°$ and Ca^{2+} from dissolution, together with the addition of $SO_4^=$, causes the precipitation of amorphous silica and gypsum:

$$CaSiO_3{\cdot}H_2O + SO_4^= + 2H^+ = CaSO_4{\cdot}2H_2O + SiO_2$$

This reaction consumes the added H^+, and the pH remains constant until the total consumption of CSH occurs. This advanced stage of alteration was never observed in the analyzed samples.

The variation in the volume of the solid phases has been calculated from the p_m values and the molar volumes included in Table 1. The formation of ettringite, a highly hydrated phase, causes an increase of up to 9% of the volume occupied by the solid phases of the cement paste (Fig. 11). As ettringite stops forming, the dissolution of portlandite causes a reduction

of −8% of the total volume of solids. The precipitation of large amounts of gypsum then increases the volume of the solids up to 35%. The dissolution of ettringite to form gypsum and gibbsite results in a small reduction in the solid volume. These changes in volume affect the resistance of the concrete producing detachments along fractures and aggregate-paste interfaces, an effect observed in altered samples. The increase of secondary porosity in the altered zones may enhance the diffusion of oxygen, the sulfide oxidation, and the transfer of $SO_4^=$ and H^+ required for alteration to progress.

According to calculations (Fig. 8), the addition of at least 3.5 mol H_2SO_4/dm^3 concrete is required to reach the alteration stage observed in the studied samples (gypsum + ettringite dissolved). On the other hand, taking into account that the amount of sulfur in the aggregates reaches 0.8 wt. % S, and assuming that all the sulfur is completely oxidized, the maximum supply of sulfuric acid from the concrete system is about 0.06 mol H_2SO_4/dm^3 concrete. Therefore, the source of H_2SO_4 is a limiting factor for alteration to progress. As a consequence, the massive alteration throughout the cement paste is not expected to occur, but rather will be limited to zones where active transport of $SO_4^=$ and H^+ takes place. Therefore, the alteration is expected to remain limited to cement-aggregate interfaces and fractures, whilst the rest of concrete will remain practically unaltered.

In conclusion, despite the fact that the chemical model described here oversimplifies the concrete system, it is a useful tool in the prediction of the behavior of the acidic alteration process. The agreement between the calculations and the observations enable us to attribute the alteration of the cement to the acidic solutions produced by the oxidation of pyrrhotite.

References

1. EH-88, Instrucción para el proyecto y la ejecución de obras de hormigón en masa ó armado. Real Decreto 824/1988 de 15 de Julio (1988).
2. A. Shayan, Cem. Concr. Res. 18, 723 (1988).
3. S. Chinchón, C. Ayora, A. Aguado, and F. Guirado, Cem. Concr. Res. 25, 1264 (1995).
4. A. Aguado (Coordinator), Estudio sobre el comportamiento de las presas de Graus y Tabescan. Convenio UPC C-1327, 1993.
5. A.C. Lasaga, J.M. Soler, T.E. Burch, and K.L Nagy, Geochim. Cosmochim. Acta 58, 2361 (1994).
6. K.L. Nagy, Reviews in Mineralogy, 31, 173 (1995).
7. R.V. Nicholson, Environmental Geochemistry of Sulfide Mine-Wastes. Short Course Handbook n. 22, J.L. Jambor and D.W. Blowes (eds.) p. 163, Mineralogical Association of Canada, 1994.
8. P.C. Singer and W. Stumm, Science 167, 1121 (1970).
9. D.W. Blowes, E.J. Reardon, J.L Jambor, and J.A. Cherry, Geochem. Cosmochem. Acta 55, 965 (1991).
10. D.A. Crerar, Geochem. Cosmochem. Acta 39, 1375 (1975).
11. D.L. Parkhurst, D.C. Thortenson, and L.N. Plummer, Water Res. Inv. 80 (1980).
12. T.J. Wolery, EQ3NR, a computer program for geochemical aqueous speciation-solubility calculations: theoretical manual, users guide and related documentation (version 7.0). Lawrence Livermore Lab., URCL-53414 (1992).
13. E.J. Reardon, Cem. Concr. Res. 20, 175 (1990).
14. V.I. Babuskin, G.M. Matveyev, and O.P. Mchedlov-Petrossyan, Thermodynamics of Silicates, p. 459, Springer-Verlag, Berlin, 1985.
15. R.A. Robie, B.S. Hemingway, and J.R. Fisher, U.S. Geol. Surv. Bull. 1452 (1979).
16. Joint Commitee on Powder Diffraction Standars. Cards 9–210 (1951) and 14–628 (1957).
17. H.M. Jennings, J. Amer. Ceram. Soc. 69, 614 (1985).
18. E.M. Gartner and H.M. Jennings, J. Amer. Ceram. Soc. 70, 743 (1987).